On the vertical families of two-dimensional tori near the triangular points of the Bicircular problem

Enric Castellà[1, 2] and Àngel Jorba[2]

June 1st, 1999

(1) Departament de Matemàtica Aplicada I, Universitat Politècnica de Catalunya, Diagonal 647, 08028 Barcelona (Spain).

(2) Departament de Matemàtica Aplicada i Anàlisi, Universitat de Barcelona, Gran Via 585, 08007 Barcelona (Spain).

E-mails: `enric@maia.ub.es`, `angel@maia.ub.es`

Abstract

This paper focuses on some aspects of the motion of a small particle moving near the Lagrangian points of the Earth-Moon system. The model for the motion of the particle is the so-called Bicircular problem (BCP), that includes the effect of Earth and Moon as in the spatial Restricted Three Body Problem (RTBP), plus the effect of the Sun as a periodic time-dependent perturbation of the RTBP. Due to this periodic forcing coming from the Sun, the Lagrangian points are no longer equilibrium solutions for the BCP. On the other hand, the BCP has three periodic orbits (with the same period as the forcing) that can be seen as the dynamical equivalent of the Lagrangian points.

In this work, we first discuss some numerical methods for the accurate computation of quasi-periodic solutions, and then we apply them to the BCP to obtain families of 2-D tori in an extended neighbourhood of the Lagrangian points. These families start on the three periodic orbits mentioned above and they are continued in the vertical (z and $\dot{z}$) direction up to a high distance. These (Cantor) families can be seen as the continuation, into the BCP, of the Lyapunov family of periodic orbits of the Lagrangian points that goes in the $(z, \dot{z})$ direction.

These results are used in a forthcoming work ([9]) to find regions where trajectories remain confined for a very long time. It is remarkable that these regions seem to persist in the real system.

Keywords: equilateral points, Lagrangian points, Bicircular problem, quasi-periodic orbits, Trojan motion, Cantor families of lower dimensional tori.

Contents

1 Introduction

Let us consider the motion of an infinitessimal particle moving in a neighbourhood of the Earth–Moon system. One of the most accurate models used to simulate this motion is the so called JPL model, and it is based on the use of the JPL ephemeris ([22]) for the position of the main bodies involved: from the ephemeris one can obtain, for a given time, the position of Earth, Moon, Sun and the planets so that we can write the vector field acting on a particle (this is a numerical vector field that it is only known for a finite time span –the time span for which the ephemeris are given–). Hence, given an initial condition, we can numerically integrate this vector field to make predictions of the subsequent motion of the particle. Of course, this integration can only be done for the time span for which the ephemeris are known.

On the other hand, there is a very well known (and simple) model for the dynamics of this problem, that is obtained under the following assumptions (i.e., simplifications): i) Let us only consider the effect of Earth and Moon; and ii) Let us assume that Earth and Moon (in this model they are usually called primaries) are punctual masses that revolve in circular orbits around their common centre of masses. The study of the motion of a small particle under the attraction of the two primaries is the so-called Restricted Three Body Problem (from now on, RTBP). It is usual to use normalized units of distance, mass and time such that the distance between the primaries, the sum of their masses and the gravitational constant are all equal to one. With these units, the period of the motion of the primaries becomes 2π. It is also common to use synodical coordinates: this is a rotating frame that has the origin at the Earth–Moon centre of masses, and the rotation is chosen in order to keep the primaries fixed on the x axis. The positive orientation of the x axis is from the smallest to the biggest primary. The z axis is ortogonal to the plane of motion and with the same orientation as the vector of angular momentum of the motion of the primaries. Finally, the y axis is taken such that the system of reference is positive definite. Defining momenta as $p_x = \dot{x} - y$, $p_y = \dot{y} + x$ and $p_z = \dot{z}$, the equations of motion can be written as an autonomous three degrees of freedom Hamiltonian system. The corresponding Hamiltonian function is

$$H_{RTBP} = \frac{1}{2}(p_x^2 + p_y^2 + p_z^2) + yp_x - xp_y - \frac{1-\mu}{r_{PE}} - \frac{\mu}{r_{PM}},$$

being $r_{PE}^2 = (x-\mu)^2 + y^2 + z^2$ and $r_{PM}^2 = (x-\mu+1)^2 + y^2 + z^2$. It is well known that this Hamiltonian has five equilibrium points, that are displayed in Figure 1. For more details see, for instance, [21] or [14].

In what follows we will focus in the equilateral points (usually called L_4 and L_5, see Figure 1). They can also be defined in a more geometrical way, as the third vertex of an equilateral triangle having the primaries as vertices. It is also well known that, for the mass parameter of the Earth–Moon case they are elliptic points. It is also possible to show that there exist a "stability region" around this point (see [4], [18], [2] and [1]). Here, by stability region we mean that initial conditions inside that region give rise to trajectories that are in the region (or very close to it) for a very long time (for instance, longer than the expected life time of the Solar system).

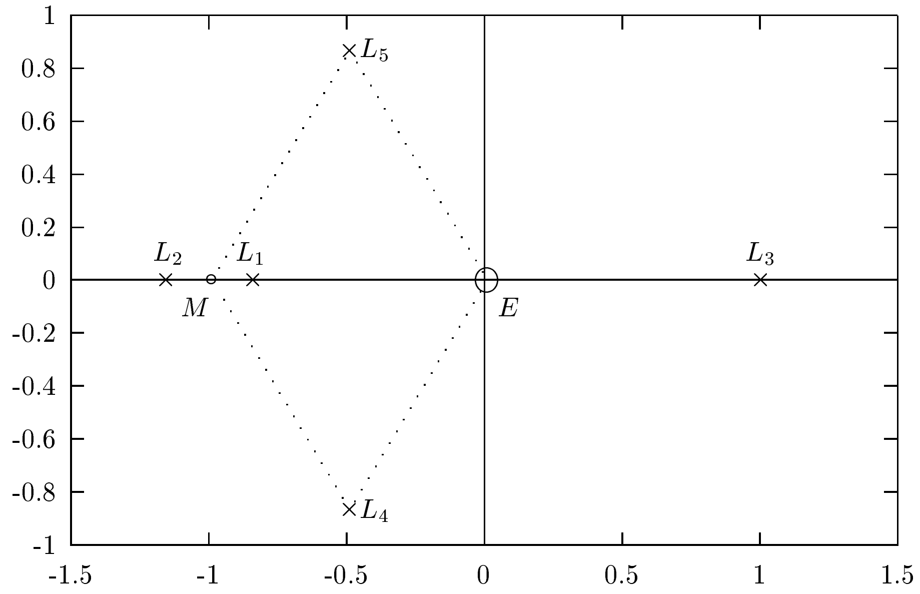

Figure 1: The five equilibrium points of the RTBP; the graphic corresponds to the Earth–Moon case, $\mu \approx 0.01215$.

On the other hand, numerical simulations using realistic models (such as the JPL ephemeris) show that the neigbourhood of the triangular points (here, we define triangular points in a geometric way, since they are not longer equilibrium points in a realistic model) is unstable (see [7], [3], [5], [6], [9]). Hence, the RTBP is not a good model to study the dynamics for the real system, since it displays a quite different qualitative behaviour.

In this paper we will use a model that is a periodic time-dependent perturbation of the RTBP, to give a first description of the dynamics close to L_4 and L_5. This model is known as the Bicircular Problem (we will refer to it as BCP) and, as far as we know, is first described in [21] (for a more exhaustive study, see [20]). For completeness, we have included a short description of the BCP in Section 2.

The results presented here are used in a forthcoming paper ([9]) to numerically compute regions (for the BCP model) where trajectories remain confined for a very long time. It is remarkable that these regions seem to persist in the JPL model, at least for time spans of 1000 years ([9]).

1.1 Families of two-dimensional tori

One of the ultimate goals of this study is to find stability regions in an extended vicinity of the triangular points of the BCP. To this end we will compute some families of lower dimensional tori. Let us explain this with more detail.

As it has been mentioned before, let us look at the BCP as a periodic time-dependent perturbation of the RTBP. Let us write a perturbing parameter ε in front of the perturbation such that when ε is 0 we have the RTBP and when ε is 1 we have the BCP (Section 2 contains the concrete details). For the moment, let us take $\varepsilon = 0$ and let us focus on the L_5 point (the same results hold for L_4 due to the symmetries of the problem). It is well known that, for the mass ratio corresponding to the Earth–Moon case, L_5 is an elliptic equilibrium point. The linear dynamics around it is described by the product of three linear oscillators: two of them are moving in the (x, y) plane, and the third one is moving on the z axis. We refer to this last one as the vertical oscillation. It can be seen that this oscillation has frequency 1 (no matter the value of the mass parameter). The well known Lyapunov centre theorem (see, for instance, [17] or [8]) ensures that there exist a family of periodic orbits of the nonlinear system that is tangent to this linear oscillation at the equilibrium point. This family can also be seen as the "nonlinear continuation" of this linear oscillation into the complete system. We will refer to this family as the vertical family of periodic orbits of L_5. It is also known that, close to the equilibrium point, the vertical family has the same stability as the point but, at some distance of L_5, this stability could change. This fact has been used in [13] to show the existence of stability regions close to L_5 for a value of the mass parameter μ for which L_5 is unstable.

Let us now take $\varepsilon > 0$ but small. Then, due to the effect of the periodic forcing, the vertical family of periodic orbits becomes a (Cantor) family of two dimensional tori. The basic frequencies of these tori are the frequency of the perturbation (the frequency of the time in the BCP) and the frequency of the corresponding periodic orbit (see [11] for more details; for a more general presentation, see [15] and [16]). We will show that the actual value of the perturbation ($\varepsilon = 1$) is big enough to produce bifurcations (see Section 2.1), such that some of these tori are hyperbolic. Nevertheless, we will show that there are some normally elliptic tori. It is also known that normally elliptic tori have a stability region around them (see [11], [12]). In this way, we will be able to determine the existence of stable regions in the BCP. The persistence of these regions for the real (JPL) model is studied in [9].

The paper is organized as follows: Section 2 describes some known results about the Bicircular model (they can be found in [20] but we include them here for completeness), Section 3 describes the numerical methods used for the computation of a single 2-D tori, Section 4 discusses the computation of a family of 2-D tori, and Section 5 contains the results obtained. Finally, the main conclusions are discussed in Section 6.

2 The Bicircular model

In this section we summarize some of the main results on the Bicircular problem (see [20] for more details).

To describe the BCP, let us assume that Earth and Moon move in circular orbits (with constant angular velocity) around their common centre of mass, and that this centre of mass moves in a circular orbit (with constant angular velocity) around the Sun, that is fixed at the origin. Note that these bodies are not moving on a true solution of the Three Body Problem.

It is very easy to write the vectorfield on an infinitessimal particle that moves under the gravitational attraction of these primaries, since the Sun is always at the origin and

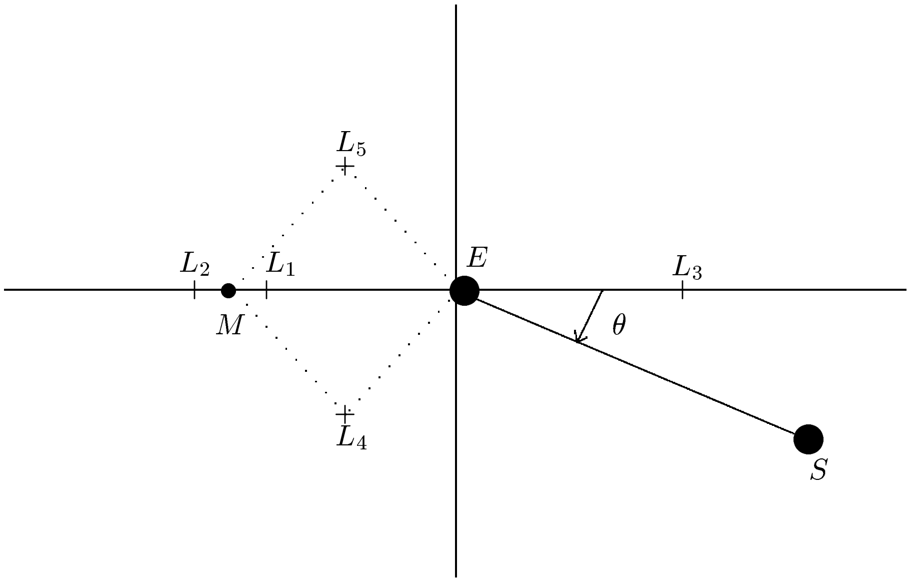

Figure 2: A schematic representation of the Bicircular problem.

the positions of Earth and Moon are given by very simple trigonometric formulae. The study of the motion of this infinitessimal particle is what is called the Bicircular problem.

To simplify the model, it is usual to take the same units and reference frame as in the RTBP: Earth and Moon are sitting on the x axis as in Figure 1, while the Sun is turning around the origin in a circular way. Then, defining the momenta as $p_x = \dot{x} - y$, $p_y = \dot{y} + x$ and $p_z = \dot{z}$, it is not difficult to check that the motion of the infinitessimal particle is described by a Hamiltonian system that depends on time in a periodic way:

$$\begin{aligned} H_{BCP} &= \frac{1}{2}\left(p_x^2 + p_y^2 + p_z^2\right) + yp_x - xp_y - \\ &\quad -\frac{1-\mu}{r_{PE}} - \frac{\mu}{r_{PM}} - \frac{m_S}{r_{PS}} - \frac{m_S}{a_S^2}\left(y\sin\theta - x\cos\theta\right), \qquad (1) \end{aligned}$$

where $r_{PE}^2 = (x-\mu)^2 + y^2 + z^2$, $r_{PM}^2 = (x-\mu+1)^2 + y^2 + z^2$, $r_{PS}^2 = (x-x_S)^2 + (y-y_S)^2 + z^2$, $x_S = a_S\cos\theta$, $y_S = -a_S\sin\theta$, and $\theta = \omega_S t$. The values used for these constants are listed in Table 1. We stress that the BCP can be written as a periodic time dependent perturbation of the RTBP:

$$H_{BCP}^{\varepsilon} = H_{RTBP} + \varepsilon\widehat{H}_{BCP}, \qquad \widehat{H}_{BCP} = -m_S\left(\frac{1}{r_{PS}} + \frac{y\sin\theta - x\cos\theta}{a_S^2}\right), \qquad (2)$$

and it is clear that $H_{BCP}^{\varepsilon=0} = H_{RTBP}$, and that $H_{BCP}^{\varepsilon=1} = H_{BCP}$.

2.1 The dynamical equivalent of the triangular points

Let us consider the BCP as a perturbation of the RTBP, as in equation (2). As the perturbation does not vanish on the equilibrium points of the RTBP, the Lagrangian

μ	$=$	0.012150581623433623	m_S	$=$	328900.54999999906
ω_S	$=$	0.925195985518289646	a_S	$=$	388.81114302335106

Table 1: Numerical values taken for the different constants of the BCP. Not all the digits are significative (they appear because the definition of these quantities involves quotients).

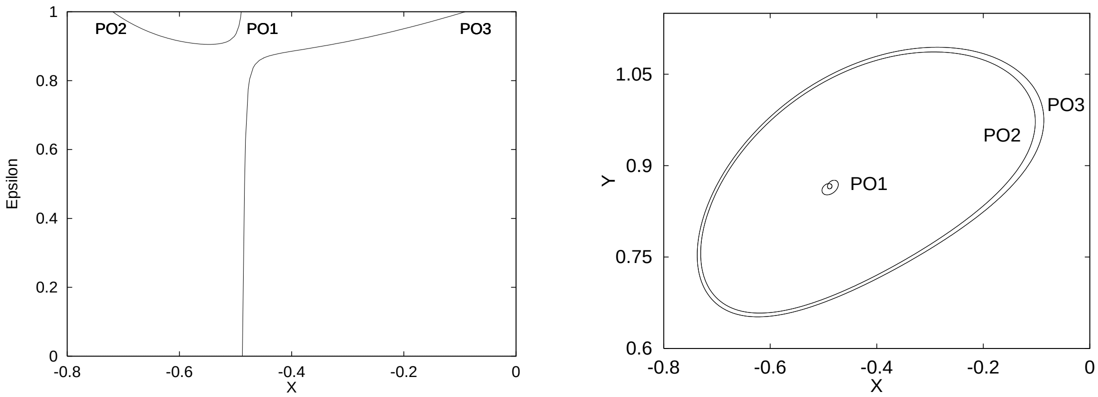

Figure 3: Left: Continuation of the periodic orbit that replaces L_5 in the BCP. Right: The three periodic orbits that appear in the left plot for $\varepsilon = 1$.

points are not longer equilibrium solutions for $\varepsilon \neq 0$. A classical result from the theory of ODE ensures that, if ε is small enough and if the linear frequencies around the point are different from $2k\pi\omega_S$, $\forall k \in \mathbb{Z}$ (we recall that ω_S is the frequency of the Sun), then the equilibrium point is replaced by a periodic orbit of frequency ω_S. This orbit goes to that point when ε goes to zero.

To compute this periodic orbit, let us define the following Poincaré map: each initial condition corresponding to $t = 0$ is mapped onto the point of the corresponding solution after one period of the time dependence, i.e., $t = 2\pi/\omega_S$. Note that the periodic orbits of frequency ω_S become fixed points of this Poincaré map. Let us call this map P_ε. It is not difficult to compute numerically P_ε and its differential, by numerical integration of the ODEs associated to (1) and the corresponding variational equations. Hence, we can apply a Newton method in order to compute the fixed points of the map. Moreover, we will use a continuation scheme with respect to the parameter ε.

Figure 3 (left) contains a diagram corresponding to this continuation. In the horizontal axis we have drawn the x coordinate of the fixed point, and in the vertical axis we have drawn the value of ε. The diagram shows the loss of uniqueness of the periodic solution when ε is close to 1. As Earth, Moon and Sun have been assumed to move in the same plane ($z = 0$), these periodic orbits are also contained in the plane $z = 0$.

Computing the eigenvalues of the monodromy matrix of the corresponding periodic orbit, it is seen that the family that is born at L_5 is always elliptic, while the other family is hyperbolic near PO1 and elliptic near PO2. In Figure 3 (right) we have drawn the (x, y) projection of the three periodic orbits that exist for $\varepsilon = 1$. The one in the centre (PO1) is

Hyperbolic eigenvalues		
PO1	1.098639921325771	0.9102163325662327

Argument of the elliptic eigenvalues			
PO1	-	2.04078041565113	0.535217643297106
PO2	0.963266156606859	0.13119540494632	0.545506883602958
PO3	0.953563380514907	0.13708329173572	0.546388819571772

Table 2: Eigenvalues of the monodromy matrices of the periodic orbits PO1, PO2 and PO3. As the hyperbolic directions correspond to eigenvalues $\lambda \in \mathbb{R}$, we display both λ and λ^{-1}. As the elliptic eigenvalues can be written as $\exp(\pm\rho\sqrt{-1})$, we only display the values ρ. In this case, the third column corresponds to the vertical oscillation.

the closest to the triangular point L_5 while the other two are quite far away. In Table 2 we have included the eigenvalues of the monodromy matrices of these three periodic orbits. The fact that PO1 is hyperbolic is responsible for the unstability of the region around L_5. So, the Bicircular model shares this property with the real Earth–Moon system.

Looking at the eigenvectors of the monodromy matrix of these periodic orbits, it is seen that all three have a complex conjugate couple of eigenvectors that is contained in the $(z, \dot{z})$ direction. They correspond to the (elliptic) complex eigenvalue whose argument is close to 0.54 (see Table 2, last column). This implies that the linearization around the periodic orbits contain solutions that can be described as the product of a vertical oscillation times the rotation along the periodic orbit (those solutions are sometimes called Lissajous orbits). From the results in [11] and [12] it follows that these Lissajous orbits can be continued into the nonlinear system: these results implies that, for each of the three periodic orbits, there exists a Cantor family of two-dimensional tori that extend those vertical oscillations. The basic frequencies of these tori are the frequency of the Sun (that is constant) and a frequency that goes to the linear normal vertical mode when the torus goes to the periodic orbit (note the similitudes of this result with the classical Lyapunov centre theorem).

For definiteness, we will call family F1 to the vertical family born from PO1, F2 the one born from PO2, and F3 the one born from PO3. In the next sections, we will compute the families F1, F2 and F3 up to high amplitudes. As we will see, this will give us insight to understand some of the features of the BCP.

3 Numerical computation of invariant curves

This section is devoted to the computation of invariant curves of a map. We will consider two different methods, that will be explained for a generic map. Later, we will use them on the Poincaré map P_ε defined before. Note that, as P_ε is a numerically defined map (we only know the result of evaluating the map at given points, as well as the corresponding

Jacobian), we can not work on any explicit representation of it (i.e., we can not perform changes of variables, etc.). So, in what follows we will assume that the only information known about the map is that it is possible to numerically evaluate its value in a given point of the phase space, as well as its differential. We will also assume, without explicit mention, that all the functions that appear here are analytic.

As usual, we will assume that the rotation number of the invariant curve is irrational, that is, that all the trajectories on the curve are dense. This is a usual hypothesis, since resonant invariant curves do not exist in a generic system (they are destroyed by arbitrarily small perturbations).

3.1 Computation of the Fourier coefficients of an invariant curve

Given an invariant curve, this first method is based on computing the Fourier coefficients of a parametrization of the curve.

3.1.1 A representation for invariant curves of a generic map

Let us consider a map f from an open set of $\mathbb{R}^n$ into itself.[1] Let us assume that this map has an invariant curve with rotation number ω, this is, we assume that there exists a map $x : \mathbb{T}^1 \to \mathbb{R}^n$ such that

$$f(x(\theta)) = x(\theta + \omega), \qquad \text{for all } \theta \in \mathbb{T}^1. \tag{3}$$

To start the discussion, let us assume that we know the rotation number of the curve we are looking for, and that we want to determine the function $x(\theta)$. Let us write $x(\theta)$ as a real Fourier series,

$$x(\theta) = a_0 + \sum_{k>0} a_k \cos(k\theta) + b_k \sin(k\theta), \qquad a_k, b_k \in \mathbb{R}^n,\ k \in \mathbb{N}.$$

As it is usual in numerical methods, we will look for a truncation of this series. So, let us fix in advance a truncation value N (the selection of the truncation value will be discussed later on), and let us try to determine (an approximation to) the $2N+1$ unknown coefficients a_0, a_k and b_k, $0 < k \le N$.

First, let us define a mesh of $2N + 1$ points on $\mathbb{T}^1$ (in all the paper we assume that the length of $\mathbb{T}^1$ is 2π),

$$\theta_j = \frac{2\pi j}{2N+1}, \qquad 0 \le j \le 2N.$$

Imposing condition (3) on the points of this mesh we obtain the system of $2N+1$ equations,

$$f(x(\theta_j)) - x(\theta_j + \omega) = 0, \qquad 0 \le j \le 2N, \tag{4}$$

that we will try to solve, by means of the Newton method, to determine the $2N + 1$ unknown Fourier coefficients.

[1] We are assuming that this map is autonomous, i.e., that it does not depend on the iterate. The case in which f depends on the iterate can be treated in a very similar way.

Hence, we consider a function F defined as follows: to each array of $2N+1$ (Fourier) coefficients $(a_0, a_1, b_1, a_2, b_2, \ldots, a_N, b_N)$, we associate the $2N+1$ values that appear in the left-hand side of (4). Note that, as each coefficient a_k (or b_k) is, in fact, an element of $\mathbb{R}^n$, the function F maps points of $\mathbb{R}^m$ into $\mathbb{R}^m$, where $m = n(2N+1)$.

Each Newton iteration requires the numerical evaluation of the function F at a given point as well as its derivatives. The evaluation of F can be easily done as follows: for a given array of Fourier coefficients it is immediate to compute, by direct evaluation of the Fourier series, the points $x(\theta_j)$ and the corresponding images by f, $f(x(\theta_j))$. Finally, the values $x(\theta_j + \omega)$ are also obtained by direct evaluation of the series.

The computation of the derivatives of F is discussed in the next section and the selection of the frequency ω and the initial guess for the Newton iterations is discussed in Section 4.

3.1.2 Computation of the Jacobian matrix

The computation of the Jacobian matrix follows from the chain rule. We recall that F maps, to each sequence of $2N+1$ (vector) Fourier coefficients, the $2N+1$ (vector) components given by

$$\left(f(x(\theta_j)) - x(\theta_j + \omega)\right)_{0 \le j \le 2N}.$$

Hence, denoting by $Df(p)$ the Jacobian of f at a given point $p \in \mathbb{R}^n$, we have that

$$\frac{\partial F}{\partial a_k} = Df(x(\theta_j)) \frac{\partial x(\theta)}{\partial a_k}(\theta_j) - \frac{\partial x(\theta + \omega)}{\partial a_k}(\theta_j).$$

Note that $Df(x(\theta_j))$ can be easily computed, and that

$$\frac{\partial x(\theta)}{\partial a_k}(\theta_j) = I_n \cos(k\theta_j), \qquad \frac{\partial x(\theta + \omega)}{\partial a_k}(\theta_j) = I_n \cos(k\theta_j + k\omega),$$

where I_n denotes the identity matrix of dimension n. Similar formulas hold for the derivatives with respect to b_k. From these formulas one can easily assemble the Jacobian matrix of F: it consist of $(2N+1) \times (2N+1)$ boxes, being each box a $n \times n$ matrix.

3.1.3 On the lack of uniqueness of the Fourier representation

It is clear that, if $x(\theta)$ is a Fourier series corresponding to an invariant curve then, for any $\varphi \in \mathbb{T}^1$, $y(\theta) \equiv x(\theta + \varphi)$ is a different Fourier series (i.e., the Fourier coefficients are different) that represents the same invariant curve as $x(\theta)$. This implies that the differential of the function F around an invariant curve will have a one-dimensional kernel. This introduces numerical difficulties when solving the linear system that appears in the Newton method.

To solve this problem we can simply add, for instance, an extra condition imposing that a component of $x(\theta)$ has a prescribed value when θ is zero (of course, there are different options). On one hand, this removes the lack of uniqueness problem and, on the other hand, this can be imposed in a very easy way: we simply add this condition as an extra equation and, as this is a linear condition, we simply add the corresponding row in the Jacobian of F.

Note that now we have to solve a linear system that has a unique solution, but it is not "squared": it has an "extra" equation. If, for instance, we are solving the linear system by means of a standard Gaussian elimination method with row pivoting, then the pivoting strategy will take care of sending to the last row the equation that is linearly dependent of the other equations. So, after the triangularization process and except by rounding errors, the last equation should read like "$0 = 0$". Hence, we can simply skip this equation and solve the triangular system in the usual way.

3.1.4 Error estimation

Assume that we have found an approximate zero of the function (4). For instance, assume that, for a given frequency ω, we have obtained Fourier coefficients such that (4) is satisfied with a tolerance of, say, 10^{-14}. As we do not have any estimation of the discretization error produced when deriving (4) from (3), we do not have information on the error of the computed invariant curve. In fact, it could be even possible that what we have computed is not an invariant curve but simply a curve containing a few invariant points.

To deal with these inconveniences, let us consider the value

$$E(x,\omega) = \max_{\theta\in\mathbb{T}^1} |f(x(\theta)) - x(\theta+\omega)|, \tag{5}$$

as an estimate of the error of the invariant curve. It is clear that x is an invariant curve with rotation number ω iff $E(x,\omega)$ is zero.

For every curve, we have approximated the value $E(x,\omega)$ by simply tabulating its value on a mesh of points on $\mathbb{T}^1$. Of course, this mesh should be finer (typically, we have used a 100 times finer mesh) than the one used to obtain (4) from (3).

When this estimate is bigger than a prescribed threshold (we have used 10^{-12}), the program automatically increases the number of Fourier coefficients and the number of discretizing points (i.e., it increases the truncation value N defined in Section 3.1.1) and recomputes the invariant curve. This process is repeated until the estimated error $E(x,\omega)$ is below 10^{-12}. In this way, all the computed invariant curves have a precision of, at least, 10^{-12} in the sense of (5).

3.2 Computation of an invariant curve by means of interpolation

In this section we will briefly describe an alternative method for computing invariant curves of maps. This method is due to C. Simó and it can be found in [19]. We refer to this reference for a more complete exposition.

3.2.1 Interpolating the Poincaré map

The goal of this method is to compute a point on the invariant curve. Let $x_0 \in \mathbb{R}^n$ be an initial condition close to the invariant curve and let us define the points $x^{(k)}$ as $f^k(x_0)$, the k-th iterate of x_0 under the map f. At this point, and to simplify the discussion, let us assume that we know the corresponding rotation number ω. Let us define T as $2\pi/\omega$, the "period" of the invariant curve (note that $T \notin \mathbb{N}$).

The main idea of this method is to define the T iterate (f^T) of the map f (as well as its Jacobian) by means of interpolation. Then, the problem is reduced to look for a fixed point of the map f^T, by means of the Newton method.

Now, let us denote by m_0 the greatest integer lower than T, and by $m_1 = m_0 + 1$. A first try to define $f^T(x_0)$ could simply be to compute the points $x^{(m_0)} = f^{m_0}(x_0)$ and $x^{(m_1)} = f^{m_1}(x_0)$, and to define $f^T(x_0)$ by linear interpolation of $x^{(m_0)}$ and $x^{(m_1)}$, $f^T(x_0) \equiv ((m_1-T)/(m_1-m_0))x^{(m_0)} + ((T-m_0)/(m_1-m_0))x^{(m_1)}$. Note that we can also compute the differential of $f^T(x_0)$ w.r.t. x_0 by simply using linear interpolation on the differentials of $f^{m_0}(x_0)$ and $f^{m_1}(x_0)$. Hence, if we know a good enough approximation to a point on the invariant curve, we can start a Newton iteration to look for the zeros of $f^T(x) - x = 0$. The result of this procedure is a single point on the invariant curve (see below for some comments about the uniqueness of the point). Of course, the point is not exactly on the invariant curve, mainly due to the poor interpolation procedure used to define $f^T(x_0)$.

A natural way of improving the accuracy is to simply use a higher order polynomial interpolation method. For this reason, we will interpolate on the points $x^{(n)}$ such that $|T-n| < \delta$, being $\delta > 1$ a prescribed value. It is important to note that the number of points we can use for the interpolation is also limited: if δ is too big, the points can be too far away from the central ones and the interpolation does not need to produce accurate results. A possibility to increase the final precision is to use iterations $x^{(n)}$ for n close to $2T$: due to the periodicity of the invariant curve, we can assume that those values correspond to the non-integer iterates $n-T$, that are close to the T iterate. Note that, as we are using a Newton method, we do not need extra precision on the differential, since the Newton method can work quite well with an approximate derivative. So, although we can use two (or more) revolutions around the invariant curve to compute a very good approximation to a point on the curve, it is usually enough to use as approximate derivative the one obtained from the interpolation on the Jacobians of the iterates corresponding to the first revolution.

One of the main difficulties of this method appears when the invariant curve has a strong hyperbolic character, since it could be impossible to come back close to the initial point after m_0 iterations. Although this is not the case here (the tori are either stable or they have a very mild unstability), this problem appears, for instance, when we are close to L_1 or L_2. The usual trick to overcome this difficulty is to use a parallel shooting technique.

As we are looking for a single point of the invariant curve, we are dealing with a problem with many solutions. To fix the point we are looking for, we will work on the section $z = 0$. It is also important to note that, with this method, we can use the rotation number as an extra unknown. In this case, to recover the uniqueness of the result, it is natural to add an extra restriction. In our case, we can achieve that by working on the section $z = 0$ and $\dot{z} = \dot{z}_0$, for a prescribed value $\dot{z}_0$ (in this case we can use $\dot{z}_0$ as a continuation parameter). This can be specially useful to find the first invariant curves of the vertical family, when the rotation numbers are unknown.

3.3 Remarks

We have described two methods for computing invariant curves of arbitrary maps of n variables. Here we want to comment which are, in our opinion, the main advantages and inconveniences of each of them.

The Fourier method has a good error estimation, allowing for an automatic selection of the truncation parameter to achieve a prescribed accuracy. Moreover, it is very well adapted for computing the normal frequencies and the hyperbolic eigenvalues of the obtained invariant curves, as it is discussed in [10]. Let us also note that the Fourier method can also be used to compute higher dimensional tori: the basic modification consists in using a mesh on $\mathbb{T}^r$ instead of a mesh on $\mathbb{T}^1$ (see Section 3.1.1), and using a Fourier series depending on r frequencies.

The interpolation method can be easily implemented, does not require the knowledge of the rotation number of the curve, and it is able to produce quite good approximations to the curves, although in some cases the accuracy can be difficult to control. Note that, depending on the Diophantine conditions of the rotation number, it can need lots of iterations before coming back near the initial condition. This can be a serious difficulty for normally hyperbolic curves (the Fourier method is less affected by the unstable character of the invariant curve, since it only requires a single iteration of the map for each point of the mesh). Moreover, the interpolation method can also be used to compute higher dimensional tori (see [19]) but, in our opinion, the Fourier method seems a better choice.

A common difficulty for both methods occurs when the curve has poles (for the time variable) in the complex plane, very close to the real line. In this case, the Fourier method needs lots of harmonics to produce good approximations (since in this case, the decay of the Fourier coefficients is very poor), and the interpolation method can present the Runge phenomenon. This is the typical situation for invariant curves close to breakdown.

In summary, their are quite complementary and can be used for efficient computation of lower dimensional tori in many situations.

4 Computation of the vertical families of invariant curves

This section starts discussing the computation of the first tori on the families (i.e., the initial guess for the Newton method as well as the corresponding frequency), and then it explains the continuation process used to obtain the complete families. For the sake of simplicity, we will focus on the case $\varepsilon = 1$. Later, we will show results for several values of ε.

4.1 First approximation of an invariant curve

There are several options for the first guess of an invariant curve. One possibility requires the normal form around the selected periodic orbit. For PO1, this normal form has already been computed in [20], and using the same software it is not difficult to obtain the normal forms around PO2 and PO3. From these normal forms it is very easy to predict the value of the frequency of an invariant curve of the vertical family, close to the periodic orbit. It is also not difficult to write a very good approximation to these invariant curves, by using the transformation that brings the Hamiltonian into its normal form.

A second possibility is to use the well-known Linsdtedt-Poincaré method, to compute the vertical family of vertical tori (see also [20]). This method has the disadvantage of being local, in the sense that it is not possible to reach high amplitudes in the vertical direction so it can not be used for the calculations we are interested in this work, but it can be useful to determine initial approximations to invariant curves (including their rotation number).

These two possibilities are able to produce very accurate approximations to invariant curves (in fact, they can produce tori of all the dimensions, but we are only interested here in the vertical family of invariant curves), and we stress that their main drawback is that they are both local methods, in the sense that they only work in a neighbourhood of the periodic orbit. As we are only interested in an initial approximation to start a Newton method, we do not need a highly accurate first guess. So, we are not going to use neither normal forms nor the Linsdtedt-Poincaré method; we will use much simpler methods instead.

First, note that an approximation to the Fourier coefficients of an invariant curve can be easily obtained from the linearization of the Poincaré map P_ε around the corresponding fixed points. To approximate the frequency, we note that it can be written as $\omega = \omega_L + \Delta\omega$, where ω_L denotes the frequency of the vertical family obtained from the linearized flow around the periodic orbit, and $\Delta\omega$ denotes the correction we must add to ω_L to obtain the frequency of the invariant curve (of course, $\Delta\omega$ depends on the amplitude of the invariant curve). Skipping resonances, any (small) value of $\Delta\omega$ corresponds to an invariant curve. One has to note, however, that there is a big difference according to the sign of $\Delta\omega$: while for one sign the invariant curves are real, for the opposite sign they are complex (this is explained in [11] and [12]). As we are implementing a Newton method to compute real invariant curves, we can use any small value for $\Delta\omega$, but with the right sign (otherwise the Newton method will converge to the fixed point instead of an invariant curve). So, we can simply choose a small value for $\Delta\omega$ and, in case it converges to the fixed point, we can try with the same value but with the opposite sign.[2] This selection of the frequency is very similar to the selection of period of one of the usual procedures to compute Lyapunov families of periodic orbits around an elliptic fixed point.

4.2 The continuation process

As it has been discussed in Section 1.1, the families of invariant curves we are interested in are Cantorian families. This means that a parametrization of these families is only defined on a set of values of the parameter of positive measure and empty interior. On the other hand it is known that, near invariant curves with a Diophantine rotation number, the

[2]Note that, even selecting the right sign for $\Delta\omega$, it is still possible to have convergence to the fixed point (because the basin of attraction of the fixed point is quite big). This problem can be overcomed by using a slightly larger value of $\Delta\omega$.

measure of the complementary of the set of values of the parameter for which the family exists is exponentially small with respect to the distance to the invariant curve (see [11] and [12] for more details). It turns out that, in most numerical computations, the Cantor family looks like a smooth family, since the "holes" of the Cantor set are so narrow that they do not show up with the usual numerical resolution. Hence, it is natural (from the numerical point of view) to deal with these families as if they were depending smoothly on the parameter. For this reason we are going to use a continuation process to compute these families. We must keep in mind that if the family has a "big gap" (i.e., a low order resonance), and we are trying to find an invariant curve inside the gap, the process should fail (more comments on this in Section 3.1.4). This is the only difference with a standard continuation, where the continuated objects are defined on an open set of the values of the parameter.

A general step of the continuation process is as follows. Let us assume that we have already computed four invariant curves. We take each invariant curve as a point in $\mathbb{R}^m$. Notice that in the Fourier method we have $m = (2N + 1)n$ (the components of a point contain the Fourier coefficients of an invariant curve), and in the interpolation method we simply have $m = 6$ which corresponds to a single point on the invariant curve. In some cases, we add an extra component to these vectors to store the rotation number of the invariant curve (in this case, the space where the continuation process takes place is $\mathbb{R}^{m+1}$). Then, we approximate the invariant curve (either in $\mathbb{R}^m$ or $\mathbb{R}^{m+1}$) by the degree three polynomial obtained from the interpolation of the last four invariant curves (the independent variable of the interpolation can be either the rotation number in the $\mathbb{R}^m$ case, or a pseudo-arc parameter in the $\mathbb{R}^{m+1}$ case). From this interpolation we can easily extrapolate the next invariant curve in the family. This approximation is then used as seed for the Newton method.

At the beginning of this continuation process, we only have one invariant curve available. We use first interpolation of degree zero to compute the second curve, then we use interpolation of degree one for the third, and interpolation of degree two to get the fourth. From this point on, we are in the general situation described in the last paragraph.

5 Results

Here we will show the families of invariant curves obtained with the methods exposed before. At this point, it should be mentioned that the extra condition used in the Newton method to overcome the lack of uniqueness problem (see Section 3.1.3) is to impose that, when the angle θ on the invariant curve is zero, the z coordinate of the curve is also zero. This condition is quite natural since all the invariant curves cross transversally the $z = 0$ plane. Hence, we can represent each invariant curve by a single (5-D) point: the intersection of the curve with the hyperplane $z = 0$.

Figure 4 displays, in the horizontal axis, the $\dot{z}$ coordinate of this point, and in the vertical axis the rotation number of the invariant curve. The plots correspond to four values of ε (denoted as Epsilon at the top of each graphic), and they show how the families of invariant tori are connected (this is clearly suggested by the left plot in Figure 3). In

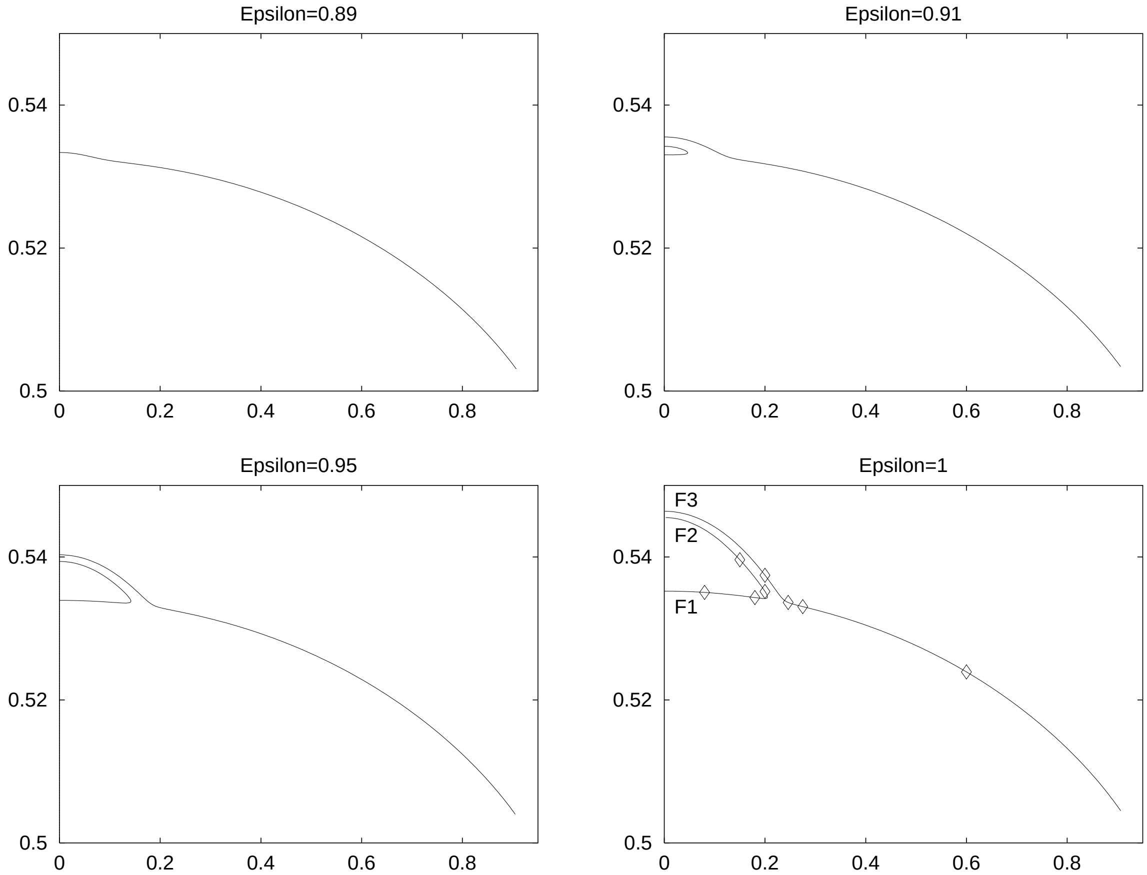

Figure 4: Vertical families of invariant tori for several values of ε. The horizontal axis shows the value of the coordinate $\dot{z}$ of the invariant curve when $z = 0$, and the vertical axis shows the corresponding rotation number. The marks on the bottom-right graphic correspond to the tori displayed in Figures 5 and 6.

particular, note that family F1 is connected with family F2.

As it has been mentioned before, these families exist for a Cantor set of vertical amplitudes. Moreover, for moderate values of the vertical amplitude, the tori in this Cantor set have the same stability as the corresponding basic periodic orbits. The holes in the Cantor set correspond to different kinds of resonances. Some of them involve the intrinsic frequencies of the torus and, hence, the torus is generically destroyed. However, there are some resonances that involve normal frequencies that do not destroy the torus but simply change its stability (giving rise to bifurcations). These resonances have been excluded from the proofs in [11] or [12], so they must take place in the complementary of the set for which the families have been proven to exist.

Hence, we expect that for small values of the vertical amplitude, most of the tori in the families F2 and F3 are elliptic, although a few of them can be hyperbolic. If the hyperbolicity is due to a high order resonance, the unstability must be so small that the tori should look as stable in a standard numerical simulation. Low order resonances can produce a quite big unstability, such that it can be easily observed in a numerical simulation. As there are no low order resonances on these families close to the basic periodic orbits, the families F2 and F3 look as stable for moderate values of the vertical amplitude. Finally, due to he hyperbolic character of the periodic orbit OP1, all the tori on F1 close to OP1 are hyperbolic, since hyperbolicity is not destroyed by resonances. A more detailed analysis of the normal stability properties of the tori in these families is contained in [10].

In figures 5 and 6 we have drawn some of the tori in these families. They have been selected in order to show the changes in their shape along the families. As expected, the main "deformations" appear for values of $\dot{z}$ between 0.2 and 0.3 (see the bottom-right plot in Figure 4).

Figure 5 contains four tori on the families F1 and F2, one in each row. The plots are numerical integrations of the flow of the BCP, made by a Runge-Kutta method of order 8, with constant stepsize equal to $(2\pi/\omega_S)/300$ (this stepsize makes the truncation errors of the integrator lower than 10^{-12}). The initial condition used is the one corresponding to the crossing of the invariant curve with the $z = 0$ plane (with positive velocity). We have plotted a point for each stepsize (i.e., 300 points per period of the Sun), and the total time span has been of 50 periods of the Sun. The first plot in each row shows the (x, y) projection of the points on the torus, the second plot contains the (x, z) projection and the third plot is the $(z, \dot{z})$ projection. The first row contains the torus (of F1) with $\dot{z} = 0.08$ (the frequency of the corresponding invariant curve in the Poincaré section is $\omega = 0.535035661376$); the second row contains the torus with $\dot{z} = 0.18$ (the frequency of the invariant curve is $\omega = 0.534313600733$); the third row shows the torus with $\dot{z} = 0.20$ (the frequency is $\omega = 0.535169441568$); and the fourth row refers to the torus (now in F2) with $\dot{z} = 0.15$ (the corresponding frequency is $\omega = 0.539605494161$). These tori have been marked in the bottom-right plot of Figure 4.

Figure 6 is similar to Figure 5, but for family F3. The first row corresponds to the torus with $\dot{z} = 0.2$ ($\omega = 0.537436421009$); the second one has $\dot{z} = 0.246$ ($\omega = 0.533632030766$); the third has $\dot{z} = 0.275$ ($\omega = 0.533046090400$); and the fourth one has $\dot{z} = 0.6$ ($\omega = 0.523915627227$). As before, they have been marked in the bottom-right plot of Figure 4.

6 Conclusions

In this paper we have used a very simple model to describe some aspects of the dynamics close to the triangular points of the Earth–Moon system. The model is good enough to predict the unstability of the region close to those points, showing that the effect of the Sun is big enough to produce bifurcations. This is already contained in a preliminar study of this model ([20]), but this work only computed the vertical family F1 up to a moderate value of the vertical amplitude. In this paper we have also computed families F2 and F3, we have shown that F1 and F2 are connected, and that F3 reaches high values of the vertical amplitude.

We want to note that family F3 is specially relevant in the study of the existence of stability regions in the Earth–Moon system: if some of the tori in this family are normally elliptic, the results in [12] ensure, under generic conditions, that there exists a region of

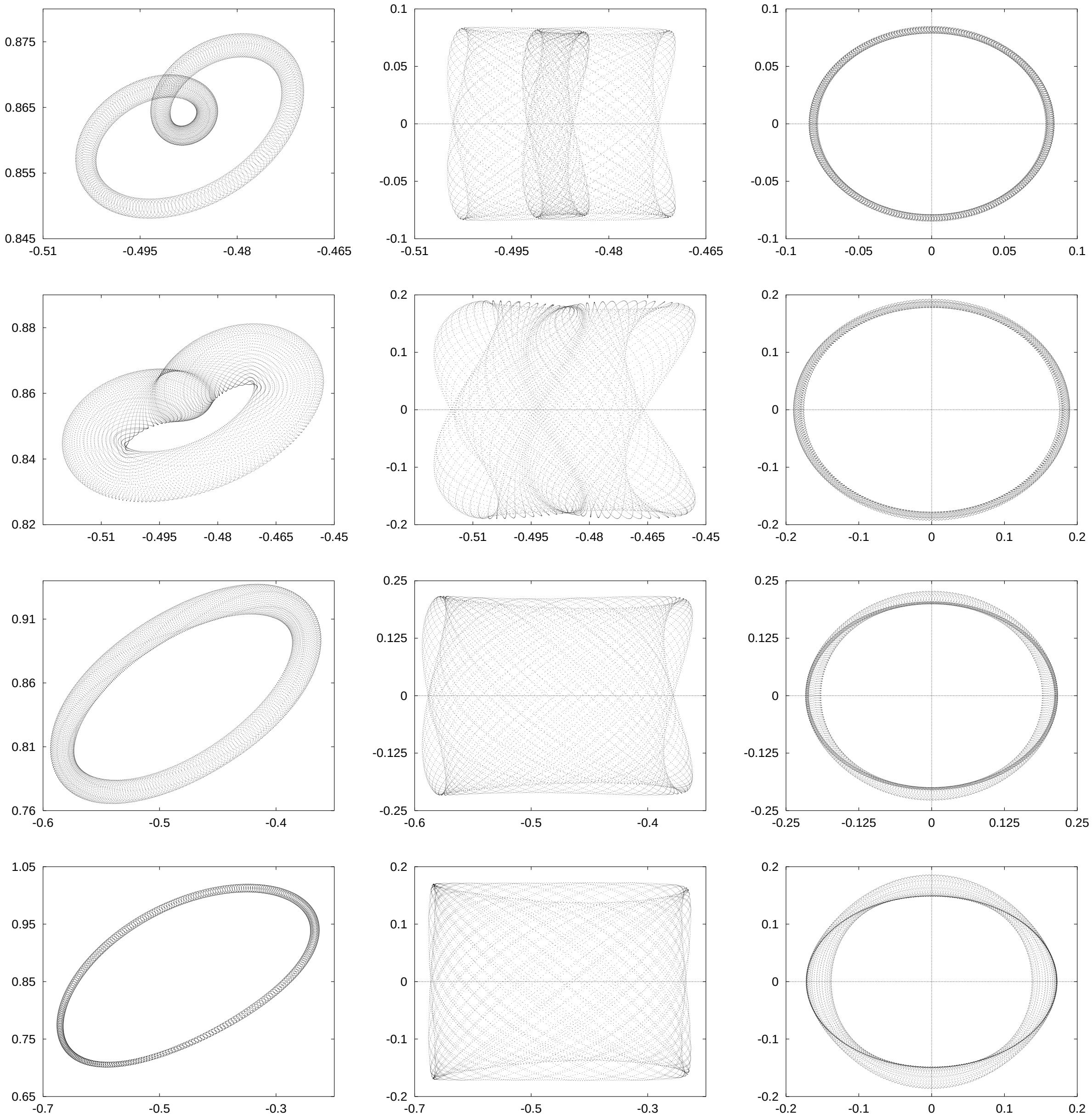

Figure 5: Tori on the families F1 and F2. See the text for details.

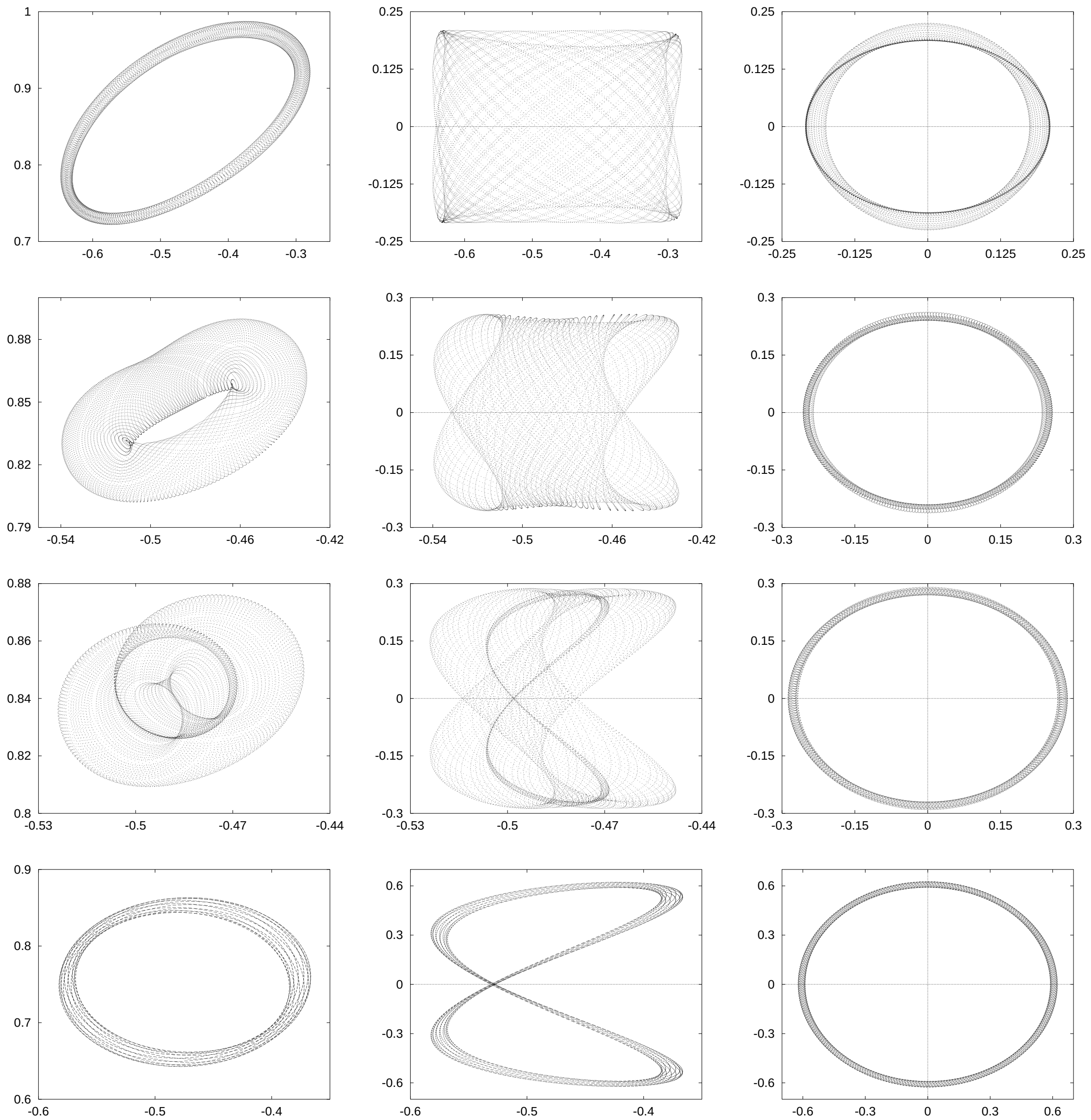

Figure 6: Tori on the family F3. See the text for details.

practical stability around them. This is exactly what happens in the BCP, as discussed in [9] and [10]. It is very remarkable that some of these regions seem to persist in the real system (see [9]). This is one of the main reasons for studying these families.

Acknowledgements

The authors want to acknowledge C. Simó for several discussions on the interpolation method, and for his comments on a previous version of this paper. The research of the second author has been supported by the Spanish grant DGICYT PB94–0215, the EC grant ERBCHRXCT940460 and the Catalan grant CIRIT 1998S0GR–00042.

References

[1] Benettin G., Fassó F., Guzzo M.: *Nekhoroshev-stability of L_4 and L_5 in the spatial Restricted Three-Body Problem*, Regular and Chaotic Dynamics (to appear).

[2] Celletti A., Giorgilli A.: *On the stability of the Lagrangian points in the spatial Restricted Three Body Problem*, Celestial Mechanics 50 (1991), pp. 31–58.

[3] Díez C., Jorba À., Simó C.: *A dynamical equivalent to the equilateral libration points of the Earth-Moon system*, Celestial Mechanics 50 (1991), pp. 13–29.

[4] Giorgilli A., Delshams A., Fontich E., Galgani L., Simó C.: *Effective stability for a Hamiltonian system near an elliptic equilibrium point, with an application to the Restricted Three Body Problem*, J. Differential Equations 77:1 (1989), pp. 167–198.

[5] Gómez G., Jorba À., Masdemont J., Simó C.: *A quasiperiodic solution as a substitute of L_4 in the Earth-Moon system*, in Proceedings of the 3rd International Symposium on Spacecraft Flight Dynamics, ESA Publications Division, ESTEC, Noordwijk, Holland (1991), pp. 35–41.

[6] Gómez G., Jorba À., Masdemont J., Simó C.: Study of Poincaré Maps for Orbits near Lagrangian Points, ESOC Contract 9711/91/D/IM(SC), Final Report (1993).

[7] Gómez G., Llibre J., Martínez R., Simó C.: Study on Orbits near the Triangular Libration Points in the Perturbed Restricted Three-Body Problem, ESOC Contract 6139/84/D/JS(SC), Final Report (1987).

[8] Henrard J.: *Lyapunov's center theorem for resonant equilibrium*, J. Differential Equations 14 (1973), pp. 431–441.

[9] Jorba À.: *A preliminary numerical study on the existence of stable motions near the triangular points of the real Earth-Moon system*, preprint (1999).

[10] Jorba À.: *Numerical computation of the normal behaviour of invariant curves of higher dimensional maps*, in progress.

[11] Jorba À., Villanueva J.: *On the Persistence of Lower Dimensional Invariant Tori under Quasi-Periodic Perturbations*, Journal of Nonlinear Science 7 (1997), pp. 427–473.

[12] Jorba À., Villanueva J.: *On the Normal Behaviour of Partially Elliptic Lower Dimensional Tori of Hamiltonian Systems*, Nonlinearity 10 (1997), pp. 783–822.

[13] Jorba À., Villanueva J.: *Numerical computation of normal forms around some periodic orbits of the Restricted Three Body Problem*, Physica D 114 (1998), pp. 197–229.

[14] Meyer K. R., Hall G. R.: Introduction to Hamiltonian Dynamical Systems and the N-Body Problem, Springer-Verlag (1992).

[15] Sevryuk M.B.: *Excitation of elliptic normal modes of invariant tori in Hamiltonian systems*, in A. Khovanskij et al. (editors): Topics in singularity theory. V.I. Arnold's 60th anniversary collection. American Mathematical Society. Transl., Ser. 2, Am. Math. Soc. 180(34), pp. 209-218 (1997).

[16] Sevryuk M. B.: *Invariant tori of intermediate dimensions in Hamiltonian systems*, Regul. Khaoticheskaya Din. 3 (1998), pp. 39–48.

[17] Siegel C.L., Moser J.: Lectures on Celestial Mechanics, Springer-Verlag (1971).

[18] Simó C.: *Estabilitat de sistemes hamiltonians*, Mem. de la Real Acad. de Ciencias y Artes de Barcelona, Vol. XLVIII, no. 7 (1989).

[19] Simó C.: *Effective computations in celestial mechanics and astrodynamics*, in V.V. Rumyantsev and A.V. Karapetyan (editors): Modern Methods of Analytical Mechanics and their Applications, CISM Courses and Lectures Vol. 387, Springer (1998).

[20] Simó C., Gómez G., Jorba À., Masdemont J.: *The bicircular model near the triangular libration points of the RTBP*, in A.E. Roy and B.A. Steves (editors): From Newton to Chaos, Plenum Press, New York (1995), pp. 343–370.

[21] Szebehely V.: Theory of Orbits, Academic Press (1967).

[22] `http://ssd.jpl.nasa.gov/horizons.html`